Vacuum 119 (2015) 34–46

Contents lists available at ScienceDirect

Vacuum

journal homepage: www.elsevier.com/locate/vacuum

Measurement of nc-Si:H film uniformity and diagnosis of plasma spatial structure produced by a very high frequency, differentially powered, multi-tile plasma source

E. Monaghan [a, *], G.Y. Yeom [b], A.R. Ellingboe [a, b, 1]

[a] Plasma Research Lab, School of Physical Sciences & NCPST, Dublin City University, Dublin 9, Ireland
[b] Department of Materials Science and Engineering, Sungkyunkwan University, Suwon 440-746, South Korea

ARTICLE INFO

Article history:
Received 27 August 2014
Received in revised form
16 March 2015
Accepted 18 March 2015
Available online 28 March 2015

Keywords:
VHF
PECVD
Multi-tile CCP
Large area
Uniformity
Nanocrystalline silicon

ABSTRACT

This paper presents the characterization of a very high frequency, differentially powered, capacitively coupled, multi-tile plasma source, MAMELUKE. Specifically, this work concentrates on the plasma enhanced chemical vapor deposition of nano-crystalline silicon suitable for application in thin film solar manufacturing. The use of a differentially-fed multi-tile source has several benefits, but imposes a spatial structure on the plasma. Sections of dielectric insulator between the differentially-fed tiles interrupt both the electrode structure and the local gas delivery to the plasma volume, both of which contribute to the gas phase chemistry uniformity profile. We investigate the affect of these factors on the plasma spatial structure by measuring the uniformity of deposited films. We examine films deposited using the MAMELUKE source focusing on the ability to produce uniform, high quality films over large areas, with high deposition rates. Spatially resolved measurements of film thickness and crystalline fraction are presented. These measurements are then used in combination with the known behaviors of very high frequency plasma systems established by previous research to draw conclusions regarding the behavior of plasma uniformity with changing process parameters. The measurements indicate that changes in the uniformity of film properties are primarily driven by gas phase chemistry effects. Changes in local gas phase chemistry are attributed to a combination of non uniformities in both the power and gas delivery in the MAMELUKE source.

1. Introduction

1.1. PECVD of nc-Si:H

Plasma enhanced chemical vapor deposition (PECVD) is a method of film deposition wildly used in many industries from the manufacture of photovoltaic and microelectronics to the coating of textiles and optics. Molecular gasses are introduced into a plasma volume and become chemically activated by plasma excitation. In addition to ionizing reactions necessary to sustain a plasma, electron-gas collisions will result in the dissociation of the source gas, giving rise to a great diversity of chemical variants. In the case of silane (SiH_4) gas which is specifically relevant to this paper, non-ionising electron-gas collisions result in the production of several radicals (SiH_3, SiH_2) and higher molecules (Si_2 H_6) that are not commonly produced at lower temperatures (200 °C). The relative densities of these chemical species depends on the various reaction rates of production and consumption. When the resulting mix of species is exposed to a substrate they encounter attractive bonding sights. Subsequent attachment of film precursors will lead to film growth upon the substrate. By controlling the plasma conditions it is possible to determine the conditions under which material is deposited, and thus partially control the properties of the deposited film. Specifically the density and energy distribution of electrons in the plasma will determine the reaction rate of each electron-gas collision process and thus the relative steady state density of each chemical species. This paper concerns it's self specifically with the PECVD of nc-Si:H. At this time significant research effort has been dedicated to the improvement of the PECVD of nc-Si:H for both solar [1–14] and display technologies [15,5,16].

* Corresponding author.
E-mail addresses: monaghe4@mail.dcu.ie (E. Monaghan), gyyeom@skku.edu (G.Y. Yeom), bert.ellingboe@dcu.ie (A.R. Ellingboe).
[1] Principal corresponding author.

http://dx.doi.org/10.1016/j.vacuum.2015.03.019
0042-207X/

In the field of thin film solar manufacturing there is significant motivation to reduce the deposition time of intrinsic nanocrystalline silicon (nc-Si:H) absorber layers in the p-i-n junction structure. These absorber layers have been successfully incorporated into single junction solar panels as well stacked multi junction cells [17,18] in conjunction with amorphous Si (a-Si:H) and/or SiGe layers. The lower band gap of nc-Si:H allows for the absorption of lower energy radiation and so junctions can be stacked to allow collection of light from a greater fraction of the electromagnetic (EM) spectrum incident on a panel. In addition nc-Si:H is not susceptible to light induced degradation a.k.a. the Staebler Wronski effect [19], which limits the long term efficiency of solar cells manufactured with only an amorphous silicon (a-Si:H) absorbing layer [20, p. 21]. However nc-Si:H has an absorption coefficient significantly lower than a-Si:H. The indirect band-gap of nc-Si:H requires a 2 particle (photon & phonon) interaction to produce an electron hole pair. This necessitates a significantly thicker absorber layer (1–2 μm) to achieve sufficient photon absorption. The necessarily long deposition time makes this manufacturing step a significant fraction of the final panel production cost. An increase in deposition rate and subsequent reduction in process time is an attractive target for possible reductions in the panel production of cost ($/W).

Higher frequency (f> 13.56 MHz) plasma processing offers the ability to produce favorable plasma conditions for the fast deposition of nc-Si:H suitable for solar manufacturing. Realizing these advantages over the large substrate areas necessity for this application has been hindered in conventional capacitively coupled plasma (CCP) source technology by “wavelength effects.” The advantages and disadvantages of high frequency excitation will be elaborated on in section 1.2, subsequently the application of high frequency excitation to PECVD processes will be explored in section 1.3.

1.2. VHF plasma

There are several advantageous to implementing very high frequency (VHF) and ultra high frequency (UHF) excitation in industrial plasma processing applications. While plasma excited by lower frequency RF tend to have Maxwellian electron energy distribution functions (EEDFs), VHF plasmas tend to have non-Maxwellian EEDFs with high densities of low energy electrons (the bulk) combined with a low population of very high energy electrons (the tail) [21,22]. The combination of these effects results in a lower average electron energy or electron temperature, T_e. When high energy electrons in “the tail” collide with atoms/molecules they have a greater probability of producing ionization. The high population of lower energy electrons will preferentially produce dissociative collisions with molecules, the lower average energy of these electrons, collisions will tend to produce low order radicals, which are often more desirable in plasma processing [23,24]. Ionization is necessary to sustain a plasma, it compensates for the continuous loss of electrons to the surrounding environment so that charged particle balance and plasma stability are maintained. The non-maxwellian EEDF produced by VHF/UHF excitation allows for a greater fraction of molecular gases to be chemically activated at a given electron density. n_e.

In addition to chemical advantages of a non-Maxwellian EEDF, the use of VHF plasma excitation reduces the average ion bombardment energy at a substrate or electrode [25,26]. The effect of excitation frequency on ion bombardment energy can be understood by examining high frequency plasma sheath behavior. This behavior can be explained to a first approximation by describing the plasma and sheath(s) as electrical components. Details given in Appendix A High ion impact energy can damage a deposited layer, specifically in nc-Si:H, high energy bombardment breaks crystalline bonds amorphizing the film [27].

Both EEDF and sheath effects described above offer potential advantages for many plasma processes including thin film silicon PECVD. Despite this, implementing VHF excitation in industrial processes has been severely limited by so called, ‘quarter wavelength effects’ [28–30]. Voltage non-uniformities on the electrode scale with the plasma loaded wavelength, $\lambda_p = \frac{\lambda_{RF}}{\sqrt{\varepsilon_p}}$, where ε_p is the plasma permittivity and λ_{RF} is the vacuum wavelength. These non uniformities become significant as the electrode diameter, d approaches a quarter of the plasma loaded wavelength. As such, with increasing substrate area the maximum excitation frequency for uniform plasma performance decreases; conversely for increasing excitation frequency the maximum area over which uniformity can be maintained is reduced. Engineering solutions using dielectric lens electrodes [31,32], ladder electrodes [33], and asymmetric sheath effects [34] have allowed for some flexibility but remain limited to excitation frequencies $\leq$100 MHz. By dividing the powered electrode into tiles and providing an isolated power supply to each tile VHF/UHF power can be used to produce plasma over much greater areas. In this paper we present the results of experiments examining the PECVD of nc-Si:H at 162 MHz using such a multi-tile source (Fig. 1).

1.3. VHF gas phase chemistry

In both solar and display applications the fractional dissociation of the feed gas used for silicon PECVD becomes critical to the process performance. The primary plasma condition in determining both the deposition rate of a process and crystalline fraction of the deposited material is the flux of both atomic hydrogen (H) and silicon containing precursors (SiH_x, $x < 4$) to the growing surface [35]. The greater the flux of precursors to the surface the higher the deposition rate of the film. However, in order to produce high quality crystalline layers at higher deposition rates the atomic hydrogen flux must also be increased. Several models have been put forward to explain this behavior. The fractional flux of hydrogen to the growing surface is thought to influence several silicon growth conditions including: 1. Increasing the surface mobility of precursors through passivation of dangling bonds [36], 2. Preferential etching of amorphous growth regions by atomic hydrogen due to the lower bond energy of amorphous material [37], and 3. Chemical annealing through local exothermic reactions such as hydrogen abstraction [38,39] ($SiH_{surface} + H_{gas} \rightarrow Si_{surface} + H_2 +$ heat). It is likely that some combination of these effects can explain the correlation between atomic hydrogen density and crystalline fraction. For each of these models, it is clear that producing both high fractional densities of film precursors ($n_{(} = SiH_x, x<4$), and atomic hydrogen (n_H) are critical to producing nanocrystalline layers at a high deposition rate. The high fractional dissociation created by VHF excitation, as described in section 0.2, is naturally conducive to favorable densities of film precursors and atomic hydrogen and thus provides beneficial conditions for high deposition rates of nc-Si:H.

Another important factor in the production of nc-Si:H films for solar applications is the relative density of various silane radicals and higher molecules. The SiH_3 radical is considered to be the primary chemical precursor for crystalline silicon growth [23]. SiH_3 has a lower surface reactivity and thus a higher surface mobility than higher order radicals (SiH_x, $x < 3$). High surface mobility allows the precursor to migrate on the substrate surface to a crystalline bonding site as opposed to an amorphous growth site. Where both crystalline and amorphous growth sights are present a crystalline site will appear more attractive to a given silicon precursor due to

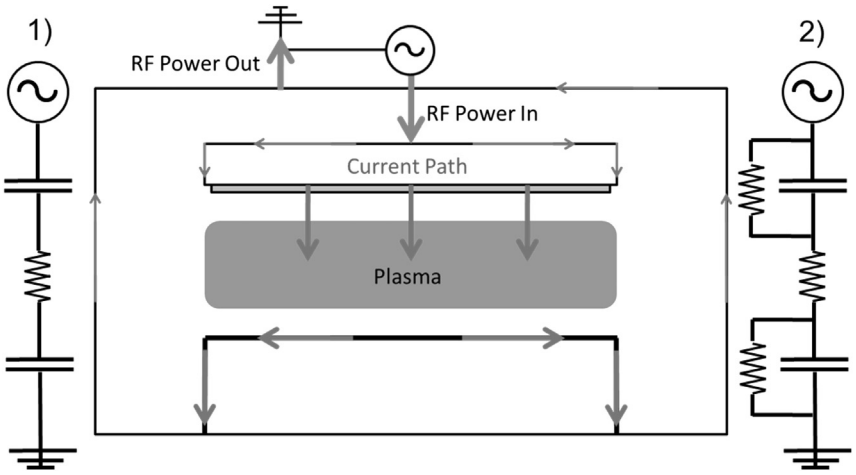

Fig. 1. A simple CCP plasma schematic showing the paths that currents take through the various elements in series, for a single point in phase. The effective electronic circuit is shown in it's most simple form to the left, 1) and with the inclusion of sheath resistors to the right, 2). The capacitive sheath elements are used to illustrate the effect of changing excitation frequency in a CCP as explained in Appendix A. The sheath resistors represent power lost to the acceleration of ions and their impact energy at the electrode.

it's lower energy state, however a precursor which impacts the substrate adjacent to an amorphous site will require sufficient kinetic/thermal energy to overcome the local potential well (local energy minima) and migrate to a crystalline site. More reactive precursors need to overcome larger (deeper) potential wells, and while typical substrate temperatures ($\approx$200 °C) allow SiH_3 radicals to overcome these potential wells, the same cannot be said for more reactive precursors. VHF plasma with an EEDF as described in 1.2 will preferentially produce low order radicals [40] at high reaction rates enabling fast deposition device quality nc-Si:H. Furthermore high order radicals (SiH_x, $x < 3$), particularly SiH_2 can lead to the formation of dust in the plasma

$$SiH_2 + Si_nH_{n+2} \rightarrow 2 + Si_{n+1}H_{n+4} \quad (1)$$

which is detrimental to process efficiency and to the production of device quality crystalline films.

2. Experiment

2.1. Plasma source

The following experiments are preformed with a 600 mm × 720 mm multi-tile CCP source, MAMELUKE [41]. The powered upper electrode is segmented into 16 tiles which are electrically insulated from each other by an inter-tile dielectric, the lower electrode and substrate holder is grounded. RF Power with a frequency of 162 MHz is supplied by an Advanced Energy Ovation 35-162 generator and split using a PSTLD Power Splitter [42]. Power is delivered from the PSTLD to the source by 8 twisted pair transmission lines; each pair of adjacent tiles are powered by a single twisted pair in a push–pull configuration (180° out of phase), these pairs will be referred to as unit cells of the multi-tile source. The design of the PSTLD ensures that each twisted pair will be driven in phase with the others (even outputs; 2, 4, 6 … are in phase as are the odd outputs 1, 3, 5 …) Fig. 2. Feed gas is supplied to the plasma through a shower head in each of the tile faces, effluent (depleted) gas is pumped through an exhaust port below the substrate holder.

By segmenting the powered electrode and powering neighboring tiles in this push–pull configuration a spatial structure is imposed on the plasma. This is caused by the relative strength of two power coupling mechanisms. Displacement current or capacitive power coupling is dominant at the tile face center, while image currents or inductive coupling is dominant at the tile edge and in the boundary between tiles. In addition the gas delivery is interrupted by the inter tile dielectric which breaks up the electrodes shower head. This in turn will contribute to gas phase chemistry non uniformities in the plasma (Fig. 3).

2.2. Measurements

In order to quantify these effects the uniformity of crystalline fraction and deposition rate are examined in films deposited at a series of process conditions. Depositions are preformed on 0.7 mm glass substrates with a transparent conducting oxide (TCO) coating. A sampling substrate 200 mm × 380 mm is placed on top of the full sized, glass "carrier" substrate in a location where it can collect deposition for several tile faces and inter tile boundaries. A masking line is drawn on the sample substrate before deposition and removed afterward so that the thickness can easily be measured with respect to the level of the bare substrate. Film thickness measurements are made with a Veco DekTak profilometer (Fig. 4).

The Raman crystalline fraction (RFC) of the material produced is determined by micro Raman spectroscopy [43–47]. The Raman spectra of deposited silicon is measured using a Kaiser Optical Systems spectrometer operated in a back-scattering configuration, at a laser wavelength of 785 nm. Each spectrum consists of the average of 2, 20 s exposures with a dark background subtraction. As

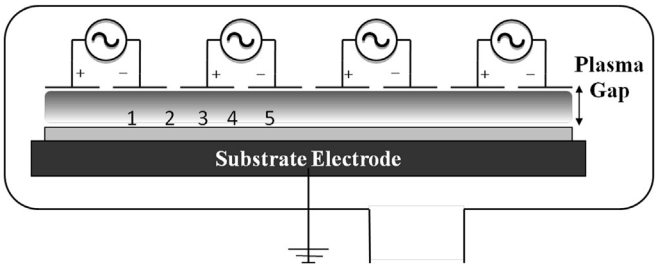

Fig. 2. The MAMELUKE source used with power divided equally between each pair of tiles. The substrate is held on a grounded movable heater. Numbers 1-5 show the location at which, measurements of the film crystalline were taken, Fig. 4. Given that PSTLD output pairs are highly isolated from each other they can be considered as independent, in phase, push–pull supplies as shown with "+" and "–" symbols representing the relative phase of each electrode at one point in phase.

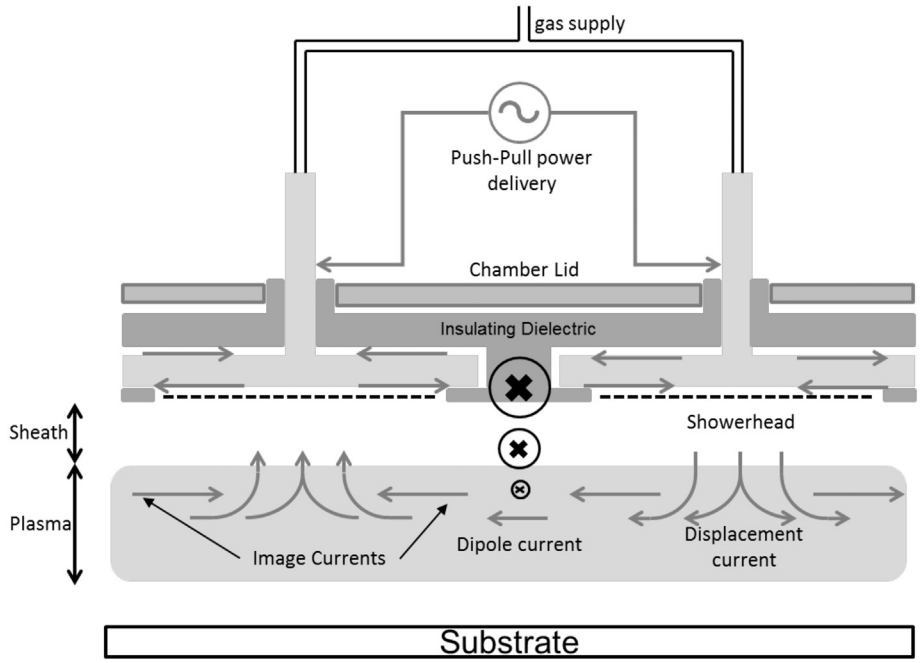

Fig. 3. Schematic of a single pair of electrodes; a "unit-cell" of the source, illustrating the non-uniformities introduced by segmenting the electrode. Arrows depict the direction of current flow at a particular point in RF phase while crosses depict the induced magnetic dipole found at a tile boundary. Different power coupling mechanisms are dominant in different spatial locations and the gas feed shower head is interrupted.

in previous studies the RCF is determined by a 3-peak fitting procedure. Three Gaussian peaks are fit to the multi-phase silicon Raman peak using the Fityk curve fitting software [48]. The stretching mode of silicon to be analyzed appears as a broad non-symmetric peak in the range of 450 cm^{-1} to 530 cm^{-1}. Three constituent peaks at 480 cm^{-1}, 510 cm^{-1} and 518 cm^{-1} are attributed to material found in the amorphous matrix, grain boundaries and nanocrystals respectively. The volumetric crystalline fraction (VCF) of the material is defined as follows:

$$X_c = \frac{I_b + I_c}{I_a + \alpha_b I_b + \alpha_c I_c} \tag{2}$$

where I_c,I_b, and I_a are the emission intensities (or the area under the respective curves) of crystalline, boundary, and amorphous peaks, respectively. In addition α_b and α_c are the relative photon cross sections for the given excitation wavelength. The relative scattering cross section in this case is the relative chance of excitation of a virtual vibrational state in crystalline material when compared to the probability of excitation in amorphous material. For example $\alpha_c = A_c/A_a$ where A_c and A_a are the absolute scattering probabilities. In all experiments detailed within this document we have assumed a relative scattering cross sections of α_b=α_c=1 for all materials giving the simplified formula

$$X_c' = \frac{I_b + I_c}{I_a + I_b + I_c} \tag{3}$$

where X_c', the Raman crystalline fraction (RCF) is related to but not equal to the VCF. This is explained as follows: While an extensive body of research investigating the absorption coefficients of amorphous, crystalline and mixed phase silicon exists [43,49,45] producing and measuring the components of mixed phase material in isolation is inherently subject to inaccuracies. This is reflected in the variance of the published figures (0.1–0.88) In addition the relative absorption coefficients can be strongly dependent on the size of nanocrystals and the Raman excitation wavelength [46]. Using relative absorption fractions of 1 gives an ease of consistency not only from measurement to measurement but also in comparison to experiments within the literature where relative scattering coefficients of 1 are also typically used. Finally by setting α_b and α_c as equal to 1 we assure that the RCF, X_c' is a lower limit for the VCF, of the examined sample.

For the results presented in section 3, it appears that a value of 0.7 for the RCF is a point of saturation. The maximum measurable RCF is a common feature for all experiments of this type, but the point of saturation will most likely be unique to a specific measurement conditions. There are 2 factors which explain the saturation i) there will always be a finite amorphous component in the spectrum which is attributable to the incubation layer and material filling gaps between individual nanocrystals and ii) selecting a relative cross section of 1 underestimates the total crystalline volume of the solid so even for small levels of amorphous material the amorphous contribution to the spectrum will be accentuated. Furthermore in films with high X_c the penetration depth of the laser

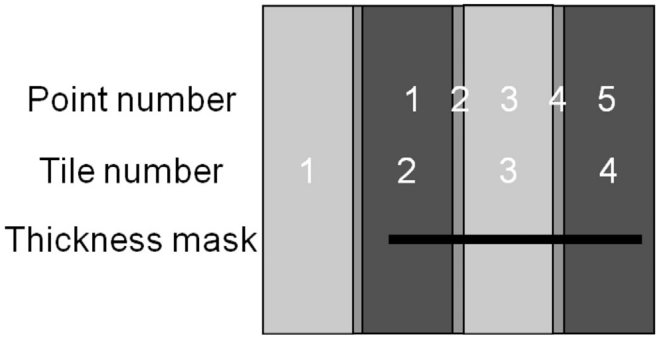

Fig. 4. A diagram showing the points at which the RCF and thickness of a film are measured relative to the electrode tiles 1-4. Tiles of a different shade are powered out of phase with each other as seen in Fig. 2.

is greater, and the fractional signal from the underlying, amorphous incubation layer is comparably over represented.

Spatially resolved measurements of RCF and thickness can reveal information on the local gas phase chemistry through correlations explained in section 2.3 and as such they will be used to qualitatively assess the nature of any non-uniformity across the plasma. The behavior of both thickness and crystalline uniformity with changing process parameters will also be considered to give further insight into the any non-uniformity in plasma parameters produced by the multi-tile plasma source configuration.

2.3. Theory & methodology

The primary experimental condition in determining the growth rate and thus the local thickness of a film is the density of dissociated or "chemically activated" silane species in the local plasma. The primary deposition condition in determining the crystalline fraction of a film is the local density of atomic hydrogen in the plasma. When considering possible process solutions for the fast production of crystalline films it is necessary to consider how each process change will affect both these conditions.

While there is a long list of process settings that can influence the plasma behavior here we have chosen to examine film properties directly with respect to 2 process settings; Forward power, P_{fwd}(W), as well as silane flow rate, Q_{SiH_4}(sccm), and indirectly - without quantitatively measuring - with respect to the gas residence time, τ_r(s). The effect of these parameters on the plasma chemistry profile in a multi-tile source can be understood in quite simple terms allowing for easier analysis of the effect of changing process settings on the plasma spatial-structure and on local/global film properties. Other experimental parameters are held constant for all depositions in this paper unless otherwise stated. The exact set-points for each of these parameters will be provided later in this section.

First we consider the effect of silane flow and power on the relative density of silane and hydrogen. The silane flow rate can simply be seen as the rate of silane delivery to the plasma and the power setting to a first approximation defines the dissociation rate. The relationship between power and dissociation rate will now be examined as well as it's importance with respect to fast crystalline growth.

- Holding other settings constant increasing the forward power will increase the rate of ionization in the plasma thus increasing the electron density

$$n_e \propto P \tag{4}$$

- Assuming that the electron temperature and EEDF shape remain approximately constant an increased electron density leads to a higher rate of dissociation. The rate at which silane is dissociated or chemically activated determines the upper limit on the deposition rate. The rate of other surface reactions such as abstraction by chemical reaction will reduce the net deposition rate, which is represented by the rate equation (5),

$$\frac{dn_{SiH_3}}{dt} \propto \alpha_1 n_{SiH_4} n'_e - n_{SiH_3}\frac{1}{d} \tag{5}$$

where n'_e is the density of electrons capable of producing the relevant reaction, α_1 and β_1 are the rate constants for dissociative and deposition processes respectively and d is the critical dimension of the plasma, in this case, the depth of the plasma between the powered electrode and substrate.

- The faster production of silane radicals encourages a high rate of film deposition which both removes silane species from the plasma, and releases several hydrogen atoms for each silicon incorporated into the film which serves as a source of hydrogen dilution not related to the hydrogen gas flow. The density of atomic hydrogen is represented by rate equation 6

$$\frac{dn_H}{dt} \propto \alpha_1 n_{SiH_4} n'_e + \alpha_2 n_{H_2} n'_e + 3\beta_1 n_{SiH_3} \tag{6}$$

Thus increasing power results in a decrease in silane containing species and an increase in atomic hydrogen density.

Parameters which are held constant during these experiments include: Gas pressure $p = 750 \pm 5$ m Torr $\approx$ 1 mbar, plasma gap, $d = 10 \pm 2$ mm; substrate temperature, $T_{sub} \approx 190 \pm 5$ °C; total gas flow, Q_{total} = 500 sccm or 250 sccm; and silane exposure, $E_{SiH_4} = 1000 \pm 10$scc. The ± numbers above represent an upper-bound in variation, not a statistically derived 1-sigma of variation.

The silane exposure setting and the motivation for its introduction warrants some explanation. The silane exposure was defined as a measure of the net amount of silicon delivered to the plasma. It is the product of the silicon flow rate (sccm) and the deposition time (mins), $E_{SiH_4} = Q_{SiH_4} t_{dep}$. We hold this parameter constant in order to achieve films of comparable thickness and as a result simplify analysis of the RCF. In addition, if the film density is assumed to be constant for all deposition conditions, any variance in the thickness of the films can provide information about the silane utilization of the plasma, which is simply a measure of the conversion efficiency from silane gas-flow to solid silicon in the film.

Previous studies have attempted to correlate film growth characteristics with atomic hydrogen density by changing the hydrogen gas dilution in the feed gas or the gas flow SiH_4:H_2 ratio. While the flow ratio does effect the atomic hydrogen density in the plasma it is not always the primary determining factor nor is it the most easily related to atomic hydrogen density. Furthermore depending on how a change in dilution ratio is achieved other effects of the changing gas flow configuration may become dominant. The depositions preformed in this study do have different levels of silane dilution but, as mentioned above it is the silane flow rate along with the RF power level that are considered to be the primary parameters which control the relative atomic hydrogen density.

3. Results and analysis

Fig. 5 contains 3 graphs. Each graph illustrates changes in the RCF uniformity of films for changing RF power, at a given silane flow rate a) 50 sccm, b) 63 sccm, and c) 75 sccm, corresponding to 10%, 12.5%, and 15% of the 500 sccm total gas flow respectively. The 5 measurement points are consistent for all RCF uniformity graphs presented in this paper and run along the long (720 mm) axis of the substrate between the center of tile 2 and the center of tile 4. The 5 spatial points of measurement are alternately located in front of three tile faces and two tile boundaries. While the RCF is measured on the substrate, we are using the source tile position as a reference for the position given that we are most interested in the effect of any plasma spatial structure on the films.

Each graph illustrates the uniformity of the RCF for 3 different levels of forward power 2600W, 3000W and 3400W which, assuming zero losses in the power transmission from generator to source, correspond to power densities of 0.60 W cm^{-2}, 0.69 W cm^{-2}, and 0.79 W cm^{-2} respectively.

Examining first Fig. 5a) films prepared at the lowest (50 sccm) silane flow over the longest (20 min) deposition, films of uniform,

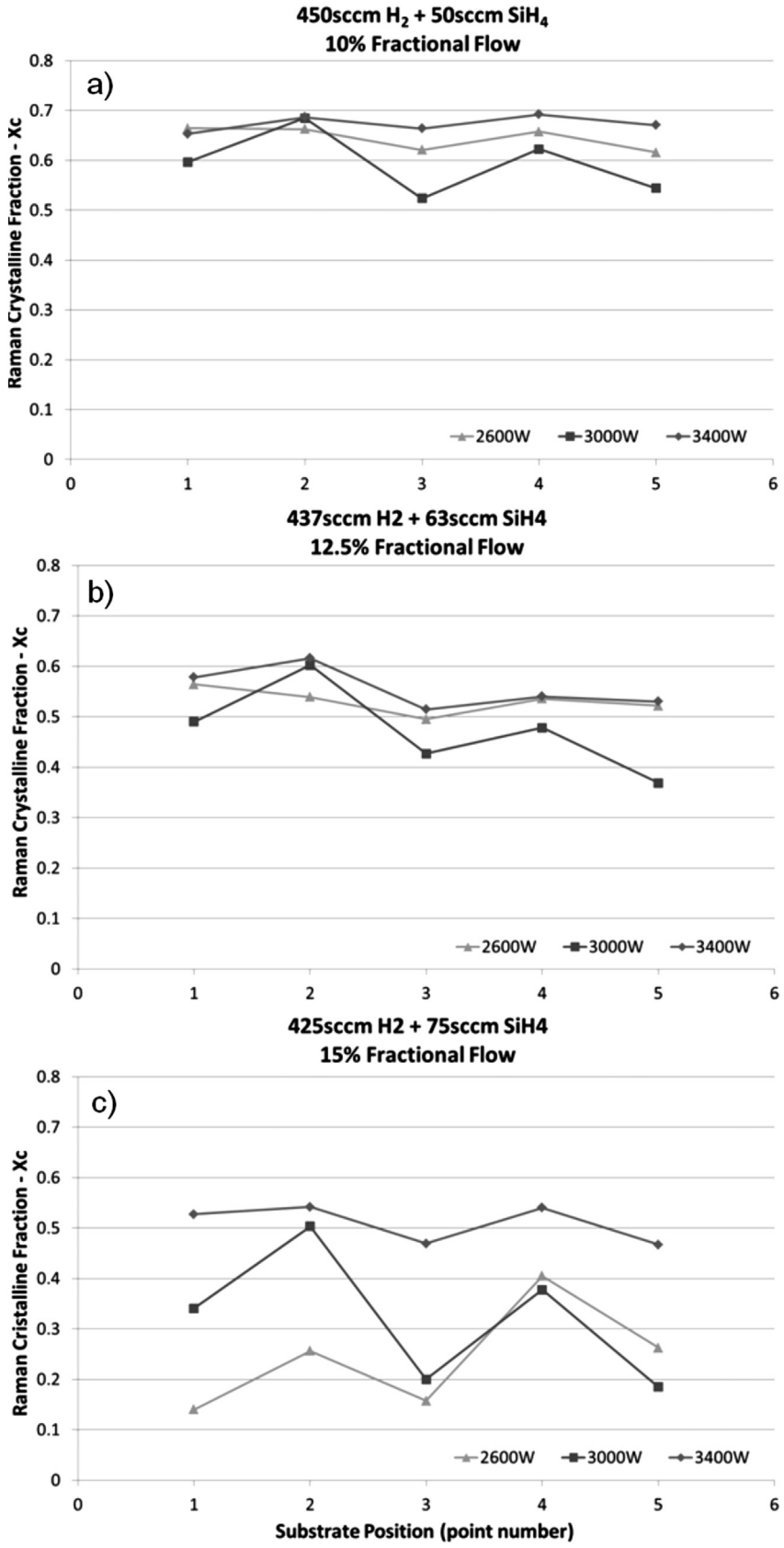

Fig. 5. Spatially resolved measurements of Raman crystalline fraction (RCF) versus RF power. All sub-graphs, a), b), c) show the measurements obtained from films deposited at 3 RF power set points, 2600 W (triangles), 3000 W (squares) and 3400 W (diamonds). Each sub graph differs by the rate of silane flow for those depositions, 50 sccm, 63 sccm & 75 sccm respectively. These silane flow rates correspond to different dilutions or fractional flows: 10%, 12.5%, 15% respectively. The total gas flow, pressure, temperature and other process parameters are held constant for all depositions.

high RCF are seen for all powers. The crystalline fraction approaches the saturation point value of 0.7, described in Section 2.2. Changing the process settings so as to increase the crystalline fraction (increasing the forward power, reducing the silane flow, or increasing the deposition time) does not discernibly increase the measured RCF beyond 0.7.

Fig. 5b) shows films prepared at an increased SiH_4 flow (63 sccm). In contrast to Fig. 5a) the average RCF of all depositions is lowered and non-uniformities in RCF are discernible between the tile center and the tile edges positions, particularly at 3000 W. This is attributed to the increase in silane flow; at the lower power settings the electron density is not sufficient to dissociate the increased flow of silane to the same degree. The silane density in the plasma is increased and the atomic hydrogen density is reduced which leads to a reduction in crystalline fraction. This trend continues in Fig. 5c), 75 sccm SiH_4 flow. The average RCF at 3400 W is only reduced slightly compared to the other flow regimes while good RCF uniformity is retained. The depositions at lower power exhibit increasing non-uniformity compared to those deposited with lower silane flow rate.

The low power RCF non-uniformities displayed in all three graphs of Fig. 5 are consistent with both plasma gas chemistry inhomogeneities and with deposition rate non-uniformities. Results from previous publications have demonstrated a strong correlation between a film's thickness and the measured RCF [41], which is strongly supported by the known growth mechanisms of nc-Si:H [50,51], specifically the development of an amorphous incubation layer early in deposition which slowly transitions to crystalline growth with increasing thickness. Given this correlation examining the thickness uniformity of these depositions helps identify the nature of plasma inhomogeneities across the multi-tile source.

Both the laser wavelength (785 nm) and the range of film thickness determine the extent to which the film thickness effects the measurement of the RCF. The penetration depth of the laser is assumed to be in excess of film thickness and as such should represent the volume averaged crystalline fraction but given that a thicker film will have a smaller fraction of their material in the incubation layer the effect cannot be completely discounted. In addition, it should be considered that films deposited with higher deposition rates often show reduced crystalline fraction. Based on this it is not trivial to predict what if any thickness non-uniformities will be displayed working from the RCF data alone. To investigate, the thickness uniformity of these depositions are plotted using the same layout in Fig. 6. The location of profilometer measurements (between tile 2 and tile 4) are displayed in Fig. 2. The thickness is measured along a strip, adjacent to the RCF measurement locations.

For all depositions it was found that the films were thicker at the tile boundary than at the tile center, which mirrors the pattern seen in the non-uniform RCF measurements. Initially this would seem to indicate that despite the long penetration depth of the 785 nm laser, the film thickness continues to have a strong influence on the measured RCF in these depositions. After further scrutiny however, it is seen that those depositions which show the greatest non-uniformity in RCF - those deposited at low power (2600 W) - show the lowest non-uniformities in thickness. In addition the thickness uniformity seems to show little or no sensitivity to the silane gas flow rate which strongly effects the RCF uniformity. It is then more likely that the RCF non-uniformities are a result of gas chemistry effects and not thickness effects.

To further emphasize the strength of correlation between the measured RCF (both the average RCF and the RCF uniformity) and the net silane flow the data in Fig. 5 is replotted in Fig. 7 such that the power is constant for each graph. In each successive graph (increasing power, a → b → c) it is found that the strength of the RCF dependence on silane flow decreases. This result further supports the idea that power and silane flow counteract each other in producing plasma chemistry desirable for crystalline growth. To clearly display the contrast of this behavior with that of the thickness uniformity Fig. 8 displays Fig. 7a) in addition to the thickness measurements of the same depositions. Despite the difference in silane flow rate, the silane exposure is kept constant and the thickness at all points remains essentially constant, which indicates efficient, consistent silane utilization for all flow rates.

It is informative to view the thickness data with a consideration for the fractional utilization of the silane gas. To accomplish this we consider the maximum achievable deposition thickness. Knowing that each deposition has been exposed to 1000 standard cubic centimeters of silane gas we can calculate the total mass of the available silicon as follows:

$$m_{SiH_4} = \frac{\rho_{SiH_4} P}{nRT} \cdot (0.874) V_{SiH_4} \tag{7}$$

where ρ_{SiH_4} is the gas density of Silane, P is the gas pressure (1 atm), n is the number of moles (=1), R is the universal gas constant ($= 82.1 \frac{cm^3 \cdot atm}{mole \cdot Kelvin}$), T is the temperature (=273.15 K), and V_{SiH_4} is the volume of silane (=1000 scc). We introduce a factor of 0.874, which is the fraction of mass associated with silicon (the 4 hydrogen atoms per molecule accounting for the remainder). This calculation gives a total deposition mass of ≈1.2525 g. Taking the density of solid silicon to be 2.329 g cm^{-3} and assuming that the substrate represents one half of the deposition area; the electrode surface making up the other half. The maximum achievable average film thickness is then calculated to be 6224 Å. We note that the maximum film thickness measured in the high-VHF MAMELUKE system is in excess of 6000A, suggesting that conversion of Silicon into film on the substrate is close to 50%.

If the effect of film thickness on the RCF uniformity can be ignored it is necessary to consider other explanations for the RCF non-uniformity at low powers and/or high silane flow. The push–pull, multi-tile configuration of the MAMELUKE source introduces a spatial structure; which induces plasma chemistry non-uniformity. We must then consider the following as possible causes for the RCF profiles.

- Changing the power set point drives changes in the relative strength of RF power coupling modes, specifically increasing the power will result in stronger coupling at electrode edges when compared to the tile faces. At higher forward powers the increased electron density leads to a decreased skin depth of the plasma, which subsequently lowers the impedance of the system to the inductive currents.
  - Increased inductive coupling will results in greater gas dissociation rates at the tile boundaries
  - Increased dissociation of SiH_4 will give rise to high deposition rated, local depletion of silane through deposition and an increased supply of hydrogen dilution.
  - These conditions are conducive to both high local deposition rate and local VCF.
- The interruption of the gas delivery shower head by inter-tile dielectric.
  - The absence of gas delivery at the tile edge means that gas entering the volume between tiles will have translated some distance through the plasma before arrival at a point on the substrate opposite the dielectric.
  - If the rate of silane dissociation is comparable to the inverse of the gas residence time this could lead to a partial depletion of the gas before arrival at the tile edge.

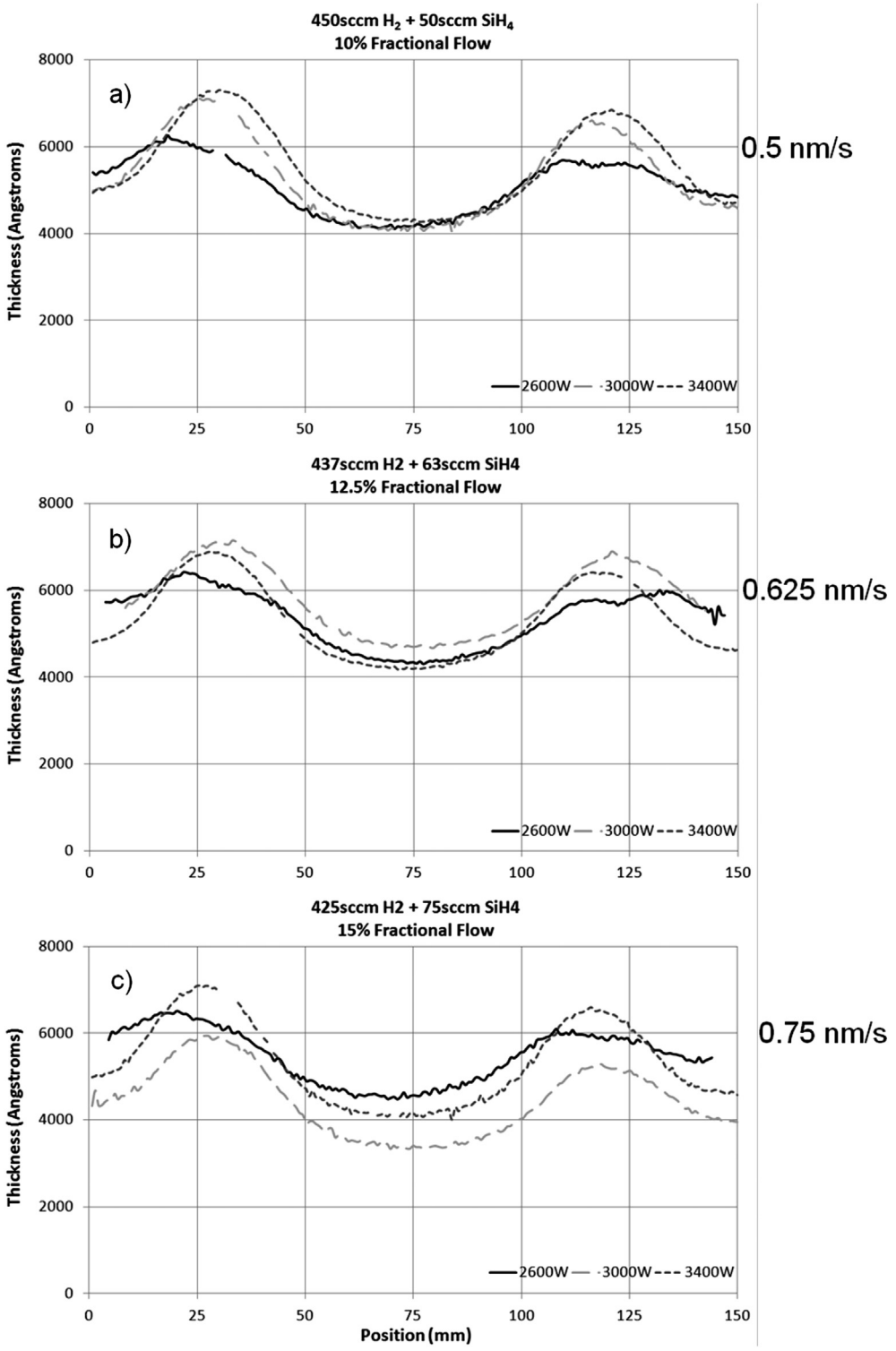

Fig. 6. Spatially resolved measurements of film thickness versus RF power. All sub-graphs, a), b), c) show the measurements obtained from films deposited at 3 RF power set points, 2600 W, 3000 W and 3400 W. Each sub graph; a, b, & c, show depositions preformed at a single silane flow rates; 50 sccm, 63 sccm, & 75 sccm respectively. These silane flow rates correspond to different silane fractional flows; 10%, 12.5%, 15% respectively. The total gas flow, pressure, temperature and other process parameters are held constant for all depositions.

– As a result the plasma in front of the tile edge will have a higher density of atomic hydrogen and a lower density of silane, a condition which is favorable for crystalline growth at the higher deposition rates experienced as a result of high power deposition through inductive coupling

Both of these possibilities are supported by the trends seen in the data. They explain the behavior of the RCF pattern when experimental settings give rise to conditions where the rate of silane dissociation is lower. As the silane flow rate is increased the crystalline fraction at the tile face drops dramatically while the at the tile edges it remains high.

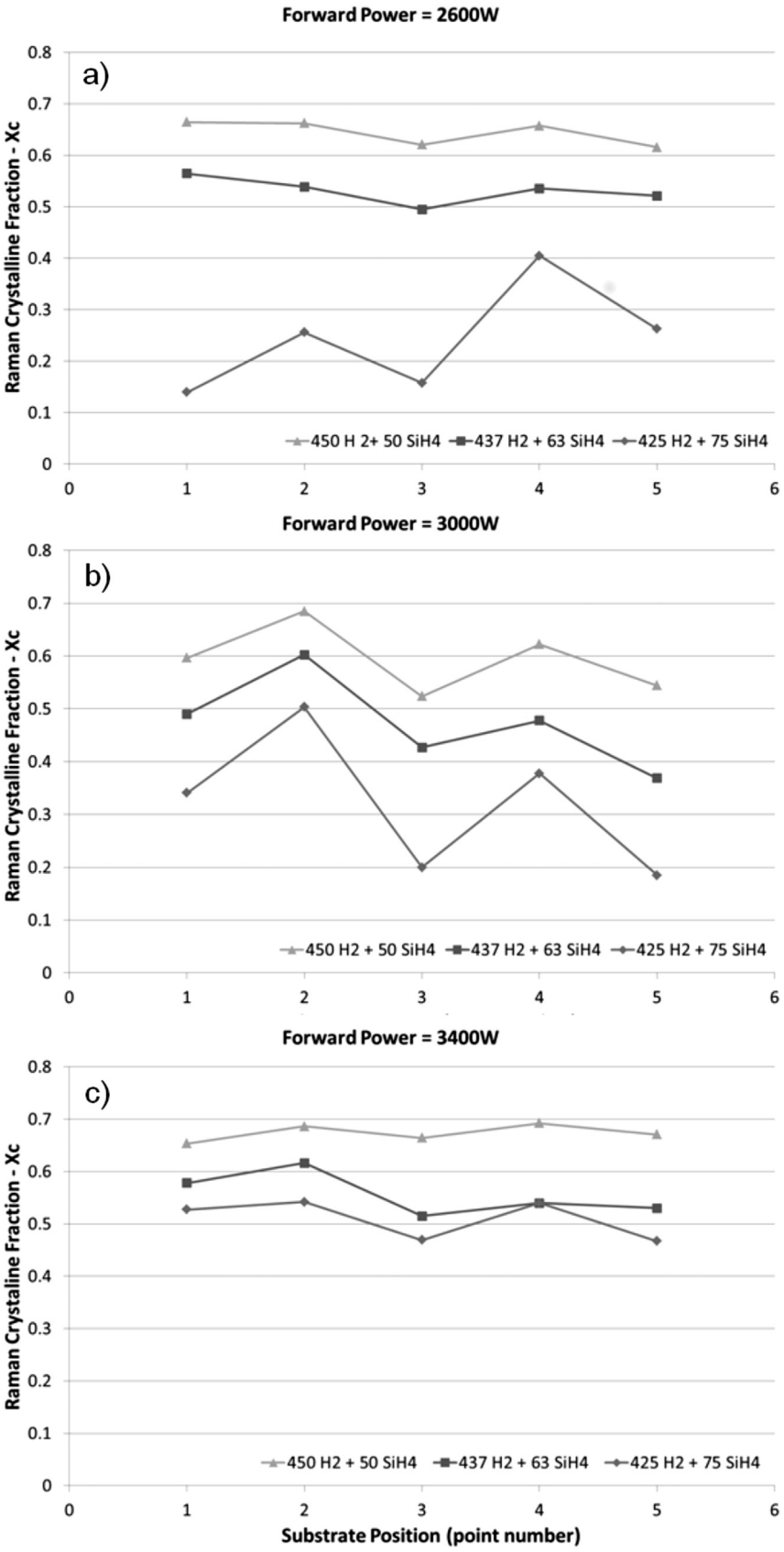

Fig. 7. Spatially resolved measurements of Raman crystalline fraction (RCF) versus the rate of silane flow. All sub-graphs, a), b), c) show the measurements obtained from films deposited at 3 silane flow rate set points, 50 sccm (triangles), 63 sccm (squares) & 75 sccm (diamonds). Each sub graph differs by the forward power set-point during the depositions. The total gas flow, pressure, temperature and other process parameters are held constant for all depositions.

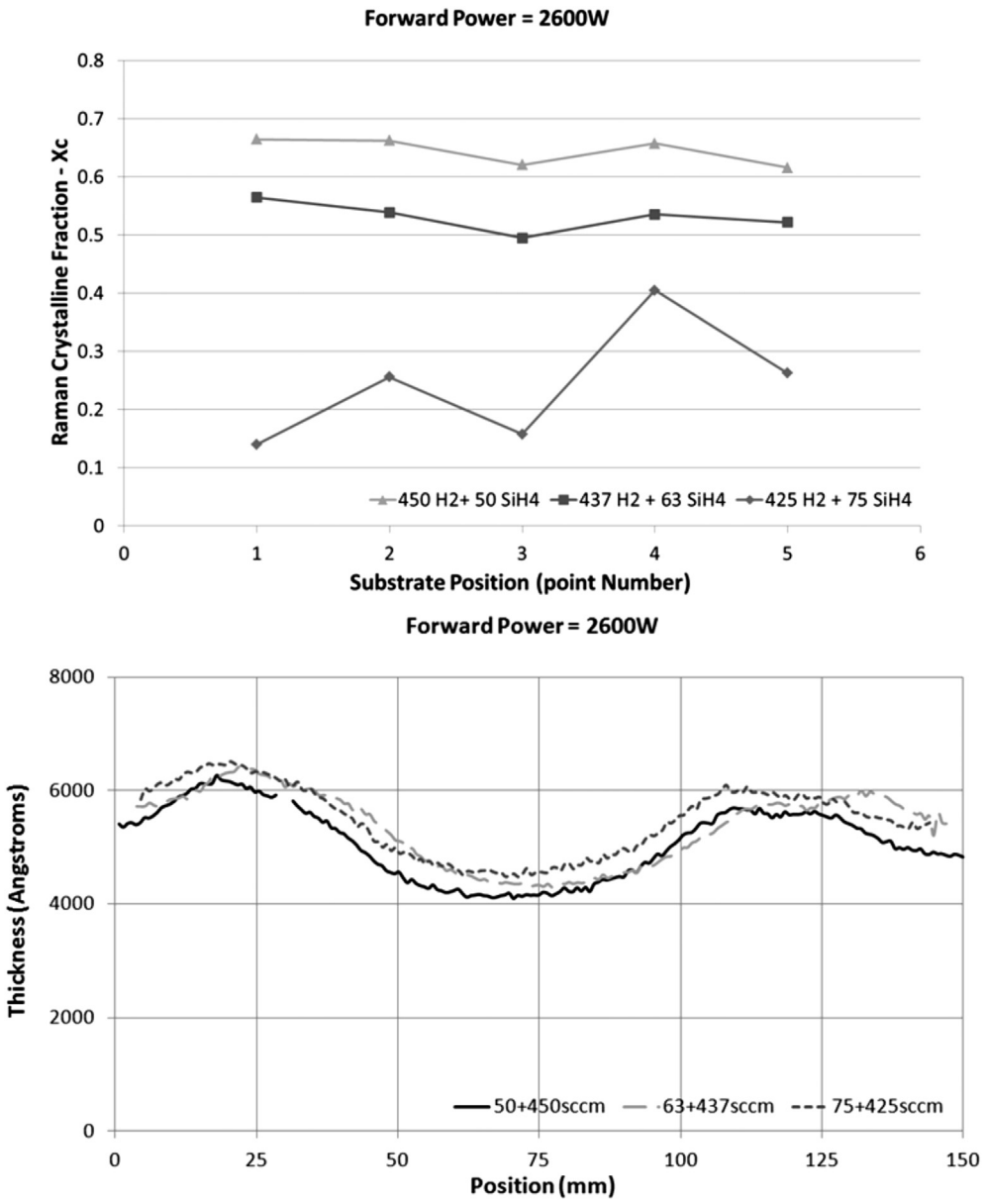

Fig. 8. RCF and thickness uniformity for depositions preformed at 2600 W forward power. The figure emphasizes the disparity between the 2 effects. For the lower silane flow depositions high levels of RCF uniformity are seen despite higher deposition at the tile edges. In addition large discrepancies are seen when comparing the depositions to each other. Significant changes in the RCF level are not reflected at all in the thickness profile which appears to be independent of both the rate of silane supply and the fractional hydrogen dilution.

The theory of high inductive coupling between this tiles is supported by the shape of deposition thickness profile and the accentuation of this non uniformity at higher powers. The theory that unequal gas delivery over small displacements can affect local gas chemistry is less easily supported. The gas pressure and the surface area of the source are such that an assumption of laminar gas flow behavior is valid, but it is not necessarily known that the residence time of a silane molecule is comparable to the inverse of the rate of dissociation. The validity of this theory is investigated experimentally by changing the residence time while maintaining the silane flow rate. To achieve this effect further depositions are preformed with reduced hydrogen flow, halving the total gas flow from 500 sccm to 250 sccm. This has the side effect of doubling the fractional flow of silane. Conventionally this reduction in the hydrogen dilution would be thought to reduce the relative atomic hydrogen density in the plasma producing a more amorphous growth regime. In Fig. 9 we see that this is not the case.

Depositions were preformed using the new flow rates at the 3 standard power set points; 2600 W, 3000 W, and 3400 W. The measurements of RCF show high crystalline fraction and high RCF uniformity for all 3 power levels. This is indicative of an increased steady state population of atomic hydrogen despite the substantial reduction in hydrogen fractional flow. The difference is most prominent at the tile faces where, previously crystalline fraction was seen to drop significantly at lower powers and high silane flow rates (Fig. 7).

This result supports the hypothesis that the time required for silane dissociation is comparable to the gas residence time, this supports the claim that local gas chemistry inhomogeneities may arise from gas delivery inhomogeneities in the MAMELUKE source.

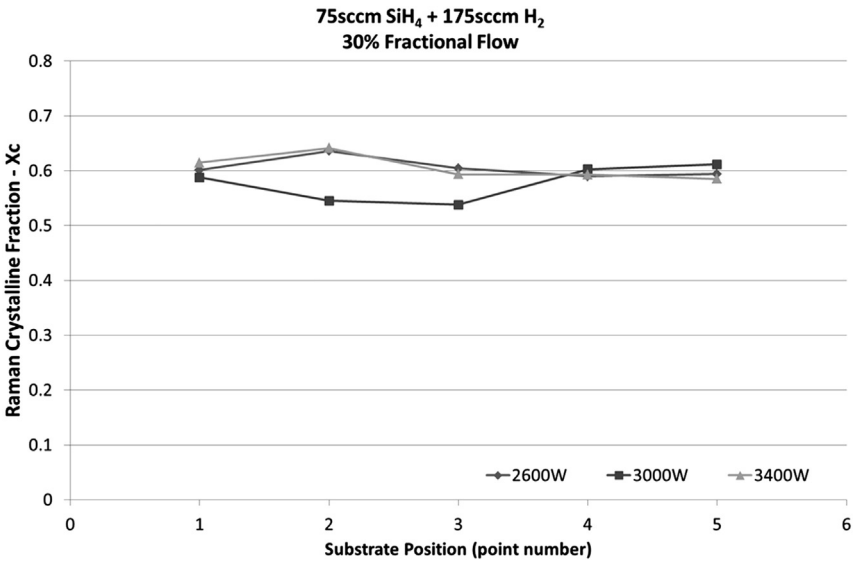

Fig. 9. Spatially resolved measurements of Raman crystalline fraction (RCF) versus forward power for depositions with increased (double) residence time compared to previous processes. Depositions were preformed at the highest rate of silane flow of 75 sccm, the increase in gas residence time is achieved by reducing the total flow which necessarily reduces the hydrogen dilution fraction from 0.85 to 0.7. Other process conditions, including pressure are the same previous depositions. Despite this the RCF remains both high and uniform for all depositions.

Specifically a reduction in the local molecular silane density and an increase in the local atomic hydrogen density at tile boundaries may directly impact the crystalline fraction but not necessarily the silicon deposition rate.

This result also supports the hypothesis that VHF excitation is capable of facilitating crystalline deposition through heavy depletion of silane. In addition this result highlights the significance of gas residence time in determining the steady state gas chemistry, specifically in achieving a heavily depleted silane population.

4. Conclusions

The VHF power used in MAMELUKE results in unique plasma processing capabilities. Specifically the source shows behavior indicating a different gas phase chemistry compared to conventional 13.56 MHz excitation. It is concluded that an increased population of high energy electrons is produced, while conserving low electron temperatures. These plasma conditions facilitate the high deposition rates observed through a high silane dissociation rate, and high depletion of the gas phase silane. In addition, there was no evidence of film amortization associated with high energy ion bombardment typically observed at higher powers. This was attributed to low sheath voltage associated with VHF excitation.

The VHF plasma which is produced by the MAMELUKE source allows for silane plasmas to be heavily depleted. As such high deposition rate nc-Si:H films can be produced with levels of hydrogen dilution significantly lower than is typical in solar manufacturing processes. In addition, when comparing depositions of a different silane flow rate the deposition thickness was found to be constant when deposition time was changed to allow for consistent silane exposure. This result indicates efficient silane utilization, or high fractional conversion of silane gas to solid silicon for all examined flow rates. These results emphasize the potential of large area VHF sources particularly in the PECVD of nc-Si:H.

Nano-crystalline silicon layers were produced at high deposition rates with a high degree of crystalline fraction uniformity. Many studies have shown this combination, but usually over small (<1 cm^2) substrate areas, this combination of material growth capabilities is not yet available in existing industrial manufacturing. Critically the results of this study demonstrate that VHF plasma and the resulting process advantages can be applied to large surface areas using multi-tile technology where conventional CCP sources encounter wavelength non-uniformities.

The deposition rate uniformity of the of the depositions was found to be effected by the power delivery profile of the push pull multi-tile source; the electron density of the plasma during these depositions was sufficient to allow dominant inductive coupling at the tile boundaries as indicated by the measured deposition thickness profiles. This thickness profile can be controlled experimentally using the process parameters, particularly in this study it has been shown to be easily controlled by the forward power. By reducing the forward power the plasma density was reduced and the plasma penetration depth increased allowing the capacitive and inductive coupling modes, and thus the layer thickness profile to become more uniform.

While deposition thickness non-uniformities were accentuated at high powers, evidence of gas chemistry inhomogeneities are accentuated in layers deposited at lower powers. At these lower powers the crystalline fraction in front of the tile face becomes lower than that at the tile edge. This is attributed to the absence of source gas delivery between the tiles. The gas flowing to the substrate locations below inter-tile boundaries is partially depleted and has a lower concentration of gas phase silane than the tile face. Under process settings where the crystalline fraction below the gas shower head is lowered the translation of the feed gas to the inter-tile boundary coincides with silane depletion and production of atomic hydrogen, this facilitates more crystalline growth at the tile boundaries.

Gas residence time in the MAMELUKE source is a more significant factor than hydrogen dilution in determining the morphology of the silicon films in the examined process space. The high dissociation rates provided by VHF excitation mean that despite reductions in hydrogen dilution, effectively doubling the silane fractional flow the fractional population of atomic hydrogen can be increased if the pumping speed is reduced to maintain constant pressure. This low dilution regime allows greater flows of silane and even higher deposition rates.

The operation of MAMELUKE in a push–pull configuration using the PSTLD increases the ease of producing plasma with full substrate coverage and negates any asymmetrical grounding paths as there is no net current into/out of the plasma. Since each of the PSTLDs output pairs are electrically isolated from each other problems with localized plasma associated with segmented electrodes are minimized.

The differential-feed on the upper electrode in addition to VHF excitation, drives RF current horizontally in the plasma (between out-of-phase tiles) rather than through the grounded substrate electrode (Fig. 3). As a result minimal RF current is driven through the sheath above the substrate. This potentially offers further process improvements by lowering ion bombardment energy and the resulting film amorphization at high power densities necessary for effective depletion of high silane flow rates.

Acknowledgments

The authors would like to thank Professor G.Y. Yeom and all members of the advanced material science and engineering group from Sungkyunkwan University (SKKU) for their valuable assistance in this research. In particular, thanks to Jeong Ho Beom for his help in using the Raman spectrometer. The authors would also like to thank GEN Ltd., Sencera International, and Advanced Energy for their various and valuable contributions to the research. This research was co-funded by Enterprise Ireland and the European Regional Development Fund (ERDF) under the National Strategic Reference Framework (NSRF) 2007–2013. Additionally, this work was supported by the Korea Institute for the Advancement of Technology and Ministry of Knowledge Economy (L-2010-1438-000), Republic of Korea. Further support was provided by The Irish Research Council's Enterprise Partnership Scheme and Intel. This and all other support received is greatly appreciated.

Appendix A. CCP circuit model

In order to explain the reduction of ion bombardment energy in VHF plasma we will consider the plasma and sheath(s) as electrical components in series with the total impedance, Z_T equaling the sum of the individual components,

$$Z_T = 2Z_S + Z_P \tag{A.1}$$

where Z_S and Z_P are the sheath impedance and plasma impedance respectively (Fig. 1). The impedance of the sheath is primarily capacitive, there is a small resistive power loss in the sheath attributable to energy gained by ions accelerated through the sheath $P_{ion} = \Gamma_{ion} e \times V_S$. For the purposes of this paper we will neglect the resistive impedance and consider only the capacitive impedance which scales inversely with frequency

$$Z_s = \frac{1}{j\omega_{RF} C} \tag{A.2}$$

where ω_{RF} is the angular frequency of the power supply, $\omega = RF 2\pi f_{RF}$. The plasma itself is primarily resistive and so will be considered to have no dependence on frequency. There is a small inductive component due to the finite mass of the electrons, $\propto j\omega L_p$ which can, again be neglected as long as the excitation frequency is less than the plasma frequency, $\omega < RF\omega_p$, where $\omega_p = \sqrt{\frac{n_e e^2}{m\varepsilon_0}} \approx 9 \times 10^8$ for industrial plasmas [52, p. 72].

Considering this simple circuit model we can evaluate the expected behavior for constant RF power but for increasing RF frequency:

- The sheath impedance (Z_s) is reduced which has the effect of decreasing the sheath voltage (V_s) and subsequently reduces energy of ions impacting the substrate.
- The net current driven between the electrodes and through the plasma (I_p) increases. The power dissipated in the plasma can be considered as ohmic heating where, the power, P_{ohm} is proportional to the square of the current driven through it, $P_{ohm} = I^2R$. The expected increase in P_{ohm} will increase the electron density and subsequently change the gas phase chemistry within the plasma.
- Both the reduction in ion bombardment energy and the increase in plasma density for a given power can be significant advantages in plasma processing applications.

References

[1] Faraji M, Gokhale S, Choudhari SM, Takwale MG, Ghaisas SV. High mobility hydrogenated and oxygenated microcrystalline silicon as a photosensitive material in photovoltaic applications. Appl Phys Lett 1992;60(26):3289–91.
[2] Meier J, Flückiger R, Keppner H, Shah A. Complete microcrystalline p-i-n solar cell—crystalline or amorphous cell behavior? Appl Phys Lett 1994;65(7):860–2.
[3] Meier J. Recent progress in micromorph solar cells. J Non-Crystalline Solids May 1998;227–230:1250–6.
[4] Shah A, Torres P, Tscharner R, Wyrsch N, Keppner H. Photovoltaic technology: the case for thin-film solar cells. Science July 1999;285:692–8 (New York, N.Y.).
[5] Perrin J, Schmitt J, Christoph, Howling A, Sansonnens L. The physics of plasma-enhanced chemical vapour deposition for large-area coating: industrial application to flat panel displays and solar cells. Plasma Phys Control Fusion Dec. 2000;42. B353+.
[6] Shah AV, Meier J, Vallat-Sauvain E, Wyrsch N, Kroll U, Droz C, et al. Material and solar cell research in microcrystalline silicon. Sol Energy Mater Sol Cells July 2003;78:469–91.
[7] Yang J, Banerjee A, Guha S. Amorphous silicon based photovoltaicsfrom earth to the final frontier. Sol Energy Mater Sol Cells July 2003;78:597–612.
[8] Shim JH, Im S, Cho NH. Nanostructural features of nc-si:h thin films prepared by pecvd. Appl Surf Sci July 2004;234:268–73.
[9] Matsui T, Matsuda A, Kondo M. High-rate microcrystalline silicon deposition for pin junction solar cells. Sol Energy Mater Sol Cells Nov. 2006;90:3199–204.
[10] Fthenakis V. Sustainability of photovoltaics: the case for thin-film solar cells. Renew Sustain Energy Rev Dec. 2009;13:2746–50.
[11] Meillaud F, Feltrin A, Dominé D, Buehlmann P, Python M, Bugnon G, et al. Limiting factors in the fabrication of microcrystalline silicon solar cells and microcrystalline/amorphous ('micromorph') tandems. Philos Mag Oct. 2009;89:2599–621.
[12] Parascandolo G, Bugnon G, Feltrin A, Ballif C. High-rate deposition of microcrystalline silicon in a large-area pecvd reactor and integration in tandem solar cells. Prog Photovolt Res Appl June 2010;18:257–64.
[13] Soderstrom T, Haug F-J, Terrazzoni-Daudrix V, Ballif C. Flexible micromorph tandem a-si/c-si solar cells. J Appl Phys 2010;107(1).
[14] Yan B, Yang J, Guha S. Amorphous and nanocrystalline silicon thin film photovoltaic technology on flexible substrates. J Vac Sci Technol A 2012;30(4).
[15] Jang J, Oh JY, Kim SK, Choi YJ, Yoon SY, Kim CO. Electric-field-enhanced crystallization of amorphous silicon. Nature Oct. 1998;395:481–3.
[16] Lee C-H, Sazonov A, Nathan A. High-mobility nanocrystalline silicon thin-film transistors fabricated by plasma-enhanced chemical vapor deposition. Appl Phys Lett May 2005;86:222106. 222106–3.
[17] Keppner H, Meier J, Torres P, Fischer D, Shah A. Microcrystalline silicon and micromorph tandem solar cells. Appl Phys A 1999;69(2):169–77.
[18] Shah AV, Vaněček M, Meier J, Meillaud F, Guillet J, Fischer D, et al. Basic efficiency limits, recent experimental results and novel light-trapping schemes in a-si:h, c-si:h and 'micromorph tandem' solar cells. J Non-Crystalline Solids June 2004;338–340:639–45.
[19] Staebler DL, Wronski CR. Reversible conductivity changes in discharge-produced amorphous si. Appl Phys Lett 1977;31(4):292–4.
[20] Hamakawa Y. Thin-film solar cells: next generation photovoltaics and its applications. Physics and Astronomy Online Library, Springer; 2004.
[21] Samukawa S, Donnelly VM, Malyshev MV. Effects of discharge frequency in plasma etching and ultrahigh-frequency plasma source for high-performance etching for ultralarge-scale integrated circuits. Jpn J Appl Phys 2000;39(4A):1583–96. Part 1.
[22] Samukawa S. Development of high-density plasma reactor for high-performance processing and future prospects. Appl Surf Sci May 2002;192:216–43.
[23] Kawasaki H, Ohkura H, Fukuzawa T, Shiratani M, Watanabe Y, Yamamoto Y, et al. Roles of **sih**$_3$ and **sih**$_2$ radicals in particle growth in rf silane plasmas. Jpn J Appl Phys 1997;36(7B):4985–8. Part 1.

[24] Hori M, Goto T. Insights into sticking of radicals on surfaces for smart plasma nano-processing. Appl Surf Sci June 2007;253:6657–71.
[25] Howling AA, Dorier, Hollenstein C, Kroll U, Finger F. Frequency effects in silane plasmas for plasma enhanced chemical vapor deposition. J Vac Sci Technol A: Vac Surfaces, Films July 1992;10:1080–5.
[26] Schwarzenbach W. Sheath impedance effects in very high frequency plasma experiments. J Vac Sci Technol A: Vac Surfaces, Films Jan. 1996;14. 132+.
[27] Johnson EV, Pouliquen S, Delattre PA, Booth JP. Hydrogenated microcrystalline silicon thin films deposited by rf-pecvd under low ion bombardment energy using voltage waveform tailoring. J Non-Crystalline Solids Sept. 2012;358:1974–7.
[28] Sansonnens L, Pletzer A, Magni D, Howling AA, Hollenstein C, Schmitt JPM. A voltage uniformity study in large-area reactors for RF plasma deposition. Plasma Sources Sci Technol May 1997;6. 170+.
[29] Lieberman MA, Booth JP, Chabert P, Rax JM, Turner MM. Standing wave and skin effects in large-area, high-frequency capacitive discharges. Plasma Sources Sci Technol Aug. 2002;11. 283+.
[30] Perret A, Chabert P, Booth JP, Jolly J, Guillon J, Ph. Ion flux nonuniformities in large-area high-frequency capacitive discharges. Appl Phys Lett 2003;83(2):243–5.
[31] Sansonnens L, Schmitt J. Shaped electrode and lens for a uniform radio-frequency capacitive plasma. Appl Phys Lett 2003;82(2):182–4.
[32] Sansonnens L, Schmidt H, Howling AA, Hollenstein C, Ellert C, Buechel A. Application of the shaped electrode technique to a large area rectangular capacitively coupled plasma reactor to suppress standing wave nonuniformity. J Vac Sci Technol A: Vac Surfaces, Films July 2006;24:1425–30.
[33] Takeuchi Y, Mashima H, Murata M, Uchino S, Kawai Y. Characteristics of very-high-frequency-excited SiH_4 plasmas using a ladder-shaped electrode. Jpn J Appl Phys May 2001;40. 3405+.
[34] Hrunski D, Mootz F, Zeuner A, Janssen A, Rost H, Beckmann R, et al. Deposition of microcrystalline intrinsic silicon by the electrical asymmetry effect technique. Vacuum 2013;87(0):114–8. Including rapid communications, original articles and a special section with papers from the Proceedings of the Eleventh International Symposium on Sputtering and Plasma Processes (ISSP 2011) 68 July 2011, Kyoto, Japan.
[35] Kroll U. From amorphous to microcrystalline silicon films prepared by hydrogen dilution using the vhf (70 mhz) gd technique. J Non-Crystalline Solids May 1998;227–230:68–72.
[36] Matsuda A. Formation kinetics and control of microcrystallite in μc-si:h from glow discharge plasma. J Non-Crystalline Solids Dec. 1983;59–60:767–74.
[37] Tsai CC, Anderson GB, Thompson R, Wacker B. Control of silicon network structure in plasma deposition. J Non-Crystalline Solids Dec. 1989;114:151–3.
[38] Nakamura K, Yoshino K, Takeoka S, Shimizu I. Roles of atomic hydrogen in chemical annealing. Jpn J Appl Phys 1995;34(2A):442–9. Part 1.
[39] Sriraman S, Agarwal S, Aydil ES, Maroudas D. Mechanism of hydrogen-induced crystallization of amorphous silicon. Nature July 2002;418:62–5.
[40] Samukawa Seiji, Nakagawa Yukito, Tsukada Tsutomu, Ueyama Hiroyuki, Shinohara Kibatsu. Lowtemperature, uniform, and highdensity plasma produced by a new ultrahighfrequency discharge with a spokewise antenna. Appl Phys Lett 1995;67(10):1414–6.
[41] Monaghan E, Michna T, Gaman C, O'Farrel D, Ryan K, Adley D, et al. Characterisation of thin film silicon films deposited by plasma enhanced chemical vapour deposition at 162mhz, using a large area, scalable, multi-tile-electrode plasma source. Thin Solid Films 2011;519:6884–6.
[42] Michna T, Ellingboe AR. Characterisation of an rf power splitter for multi-tile pecvd systems application. Curr Appl Phys Sept. 2011;11:S9–11.
[43] Iqbal Z, Veprek S. Raman scattering from hydrogenated microcrystalline and amorphous silicon. J Phys C: Solid State Phys Jan. 1982;15. 377+.
[44] Smit C, van Swaaij, Donker H, Petit AMHN, Kessels WMM, van de Sanden MCM. Determining the material structure of microcrystalline silicon from raman spectra. J Appl Phys 2003;94(5):3582–8.
[45] Han D, Lorentzen JD, Wolf WJ, Mcneil LE, Wang Q. Raman study of thin films of amorphous-to-microcrystalline silicon prepared by hot-wire chemical vapor deposition. J Appl Phys 2003;94(5):2930–6.
[46] Ledinsky M, Vetushka A, Stuchlik J, Mates T, Fejfar A, Kocka J, et al. Crystallinity of the mixed phase silicon thin films by raman spectroscopy. J Non-Crystalline Solids May 2008;354:2253–7.
[47] Strahm B, Hollenstein C, Howling AA. Uniformity of silicon microcrystallinity in large area RF capacitive reactors. Prog Photovolt Res Appl Dec. 2008;16:687–91.
[48] Wojdyr M. Fityk: a general-purpose peak fitting program. J Appl Cryst Oct. 2010;43:1126–8.
[49] Ossadnik C, Vepřek S, Gregora I. Applicability of raman scattering for the characterization of nanocrystalline silicon. Thin Solid Films Jan. 1999;337:148–51.
[50] Houben L, Luysberg M, Hapke P, Carius R, Finger F, Wagner H. Structural properties of microcrystalline silicon in the transition from highly crystalline to amorphous growth. Philos Mag A 1998;77(6):1447–60.
[51] Sauvain EV, Kroll U, Meier J, Shah A, Pohl J. Evolution of the microstructure in microcrystalline silicon prepared by very high frequency glow-discharge using hydrogen dilution. J Appl Phys Mar. 2000;87:3137–42.
[52] Chapman B. Glow discharge processes: sputtering and plasma etching. A Wiley-Interscience publication, Wiley; 1980.